

Hyperbolic metamaterial antenna for second-harmonic generation tomography

Paulina Segovia,^{1,2,5} Giuseppe Marino,^{1,5} Alexey V. Krasavin,^{1,5} Nicolas Olivier,¹
Gregory A. Wurtz,^{1,3} Pavel A. Belov,⁴ Pavel Ginzburg,^{1,2,*} and Anatoly V. Zayats¹

¹Department of Physics, King's College London, Strand, London WC2R 2LS, UK

²Currently with the School of Electrical Engineering, Tel Aviv University, Tel Aviv 69978, Israel

³Currently with the Department of Physics, University of North Florida, Jacksonville Florida 32224, USA

⁴National Research University of Information Technologies, Mechanics and Optics (ITMO), St. Petersburg 197101, Russia

⁵Contributed equally

* pavel.ginzburg@kcl.ac.uk

Abstract: The detection and processing of information carried by evanescent field components are key elements for subwavelength optical microscopy as well as single molecule sensing applications. Here, we numerically demonstrate the potential of a hyperbolic medium in the design of an efficient metamaterial antenna enabling detection and tracking of a nonlinear object, with an otherwise hidden second-harmonic signature. The presence of the antenna provides 10^3 -fold intensity enhancement of the second harmonic generation (SHG) from a nanoparticle through a metamaterial-assisted access to evanescent second-harmonic fields. Alternatively, the observation of SHG from the metamaterial itself can be used to detect and track a nanoparticle without a nonlinear response. The antenna allows an optical resolution of several nanometers in tracking the nanoparticle's location via observations of the far-field second-harmonic radiation pattern.

©2015 Optical Society of America

OCIS codes: (160.3918) Metamaterials; (180.4315) Nonlinear microscopy; (190.2620) Harmonic generation and mixing.

References and links

1. M. Born and E. Wolf, *Principles of Optics: Electromagnetic Theory of Propagation, Interference and Diffraction of Light* (Cambridge University, 1999).
2. Z. Zalevsky and D. Mendlovic, *Optical Superresolution* (Springer, 2004).
3. V. A. Podolskiy and E. E. Narimanov, "Near-sighted superlens," *Opt. Lett.* **30**(1), 75–77 (2005).
4. J. B. Pendry, "Negative refraction makes a perfect lens," *Phys. Rev. Lett.* **85**(18), 3966–3969 (2000).
5. Z. Jacob, L. V. Alekseyev, and E. Narimanov, "Optical hyperlens: Far-field imaging beyond the diffraction limit," *Opt. Express* **14**(18), 8247–8256 (2006).
6. W. Yan, N. A. Mortensen, and M. Wubs, "Hyperbolic metamaterial lens with hydrodynamic nonlocal response," *Opt. Express* **21**(12), 15026–15036 (2013).
7. L. Ferrari, C. Wu, D. Lepage, X. Zhang, and Z. Liu, "Hyperbolic metamaterials and their applications," *Prog. Quantum Electron.* **40**, 1–40 (2015).
8. H. N. S. Krishnamoorthy, Z. Jacob, E. Narimanov, I. Kretzschmar, and V. M. Menon, "Topological transitions in metamaterials," *Science* **336**(6078), 205–209 (2012).
9. A. N. Poddubny, P. A. Belov, P. Ginzburg, A. V. Zayats, and Y. S. Kivshar, "Microscopic model of Purcell enhancement in hyperbolic metamaterials," *Phys. Rev. B* **86**(3), 035148 (2012).
10. W. Yan, M. Wubs, and N. A. Mortensen, "Hyperbolic metamaterials: nonlocal response regularizes broadband supersingularity," *Phys. Rev. B* **86**(20), 205429 (2012).
11. A. V. Kabashin, P. Evans, S. Pastkovsky, W. Hendren, G. A. Wurtz, R. Atkinson, R. Pollard, V. A. Podolskiy, and A. V. Zayats, "Plasmonic nanorod metamaterials for biosensing," *Nat. Mater.* **8**(11), 867–871 (2009).
12. Z. Liu, H. Lee, Y. Xiong, C. Sun, and X. Zhang, "Far-field optical hyperlens magnifying sub-diffraction-limited objects," *Science* **315**(5819), 1686 (2007).
13. D. Lu and Z. Liu, "Hyperlenses and metalenses for far-field super-resolution imaging," *Nat. Commun.* **3**, 1205 (2012).

14. A. Schilling, J. Schilling, C. Reinhardt, and B. Chichkov, "A superlens for the deep ultraviolet," *Appl. Phys. Lett.* **95**(12), 121909 (2009).
15. A. V. Zayats and V. Sandoghdar, "Apertureless near-field optical microscopy via local second-harmonic generation," *J. Microsc.* **202**(1), 94–99 (2001).
16. S. Takahashi and A. V. Zayats, "Near-field second-harmonic generation at a metal tip apex," *Appl. Phys. Lett.* **80**(19), 3479–3481 (2002).
17. P. J. Campagnola and L. M. Loew, "Second-harmonic imaging microscopy for visualizing biomolecular arrays in cells, tissues and organisms," *Nat. Biotechnol.* **21**(11), 1356–1360 (2003).
18. L. Sacconi, D. A. Dombeck, and W. W. Webb, "Overcoming photodamage in second-harmonic generation microscopy: real-time optical recording of neuronal action potentials," *Proc. Natl. Acad. Sci. U.S.A.* **103**(9), 3124–3129 (2006).
19. I. I. Smolyaninov, A. V. Zayats, and C. C. Davis, "Near-field second harmonic generation from a rough metal surface," *Phys. Rev. B* **56**(15), 9290–9293 (1997).
20. A. V. Zayats, T. Kalkbrenner, V. Sandoghdar, and J. Mlynek, "Second-harmonic generation from individual surface defects under local excitation," *Phys. Rev. B* **61**(7), 4545–4548 (2000).
21. D. de Ceglia, M. A. Vincenti, S. Campione, F. Capolino, J. W. Haus, and M. Scalora, "Second-harmonic double-resonance cones in dispersive hyperbolic metamaterials," *Phys. Rev. B* **89**(7), 075123 (2014).
22. A. D. Neira, N. Olivier, M. E. Nasir, W. Dickson, G. A. Wurtz, and A. V. Zayats, "Eliminating material constraints for nonlinearity with plasmonic metamaterials," *Nat. Commun.* **6**, 7757 (2015).
23. W. Dickson, S. Beckett, C. McClatchey, A. Murphy, D. O'Connor, G. A. Wurtz, R. Pollard, and A. V. Zayats, "Hyperbolic polaritonic crystals based on nanostructured nanorod metamaterials," *Adv. Mater.* **27**(39), 5974–5980 (2015).
24. H. J. Elser, R. Wangberg, V. A. Podolskiy, and E. E. Narimanov, "Nanowire metamaterials with extreme optical anisotropy," *Appl. Phys. Lett.* **89**(26), 261102 (2006).
25. N. Vasilantonakis, M. E. Nasir, W. Dickson, G. A. Wurtz, and A. V. Zayats, "Bulk plasmon-polaritons in hyperbolic nanorod metamaterial waveguides," *Laser Photonics Rev.* **9**(3), 345–353 (2015).
26. J. Stratton, *Electromagnetic Theory* (McGraw-Hill, 1941).
27. G. Bachelier, I. Russier-Antoine, E. Benichou, C. Jonin, and P.-F. Brevet, "Multipolar second-harmonic generation in noble metal nanoparticles," *J. Opt. Soc. Am. B* **25**(6), 955–960 (2008).
28. J. I. Dadap, J. Shan, K. B. Eisenthal, and T. F. Heinz, "Second-harmonic Rayleigh scattering from a sphere of centrosymmetric material," *Phys. Rev. Lett.* **83**(20), 4045–4048 (1999).
29. J. I. Dadap, J. Shan, and T. F. Heinz, "Theory of optical second-harmonic generation from a sphere of centrosymmetric material: small-particle limit," *J. Opt. Soc. Am. B* **21**(7), 1328–1347 (2004).
30. E. V. Makeev and S. E. Skipetrov, "Second harmonic generation in suspensions of spherical particles," *Opt. Commun.* **224**(1-3), 139–147 (2003).
31. G. Marino, P. Segovia, A. V. Krasavin, P. Ginzburg, N. Olivier, G. A. Wurtz, and A. V. Zayats, "Second-harmonic generation from hyperbolic plasmonic nanorod metamaterial slab," <http://arxiv.org/abs/1508.07586>.
32. P. V. Kapitanova, P. Ginzburg, F. J. Rodríguez-Fortuño, D. S. Filonov, P. M. Voroshilov, P. A. Belov, A. N. Poddubny, Y. S. Kivshar, G. A. Wurtz, and A. V. Zayats, "Photonic spin Hall effect in hyperbolic metamaterials for polarization-controlled routing of subwavelength modes," *Nat. Commun.* **5**, 3226 (2014).
33. D. de Ceglia, M. A. Vincenti, C. De Angelis, A. Locatelli, J. W. Haus, and M. Scalora, "Role of antenna modes and field enhancement in second harmonic generation from dipole nanoantennas," *Opt. Express* **23**(2), 1715–1729 (2015).
34. C. Forestiere, G. Iadarola, G. Rubinacci, A. Tamburrino, L. Dal Negro, and G. Miano, "Surface integral formulations for the design of plasmonic nanostructures," *J. Opt. Soc. Am. A* **29**(11), 2314–2327 (2012).

1. Introduction

A key challenge in microscopy is spatial resolution, mediating the relation between real features of an object and its observed image. In optical microscopy, a complete set of electromagnetic modes including the evanescent ones is required to reconstruct a perfect image. Evanescent modes, however, decay in the vicinity of the object before being detected in the far-field, giving rise to the diffraction limit [1]. Among various approaches for resolution improvement [2], the use of nanostructured composites (metamaterials) is beneficial, enabling efficient manipulation of evanescent fields components in order to reconstruct the image of an object with the resolution limited only by a particular realization of the metamaterial, e.g., its inherent material losses [3]. While superlenses [4] do not change the decaying nature of evanescent components, lenses made with materials exhibiting hyperbolic dispersion (hyperlenses) [5,6] convert them in propagating modes detectable in the far-field. This near-to-far field transformation is enabled by the hyperbolic dispersion of the medium which occurs in uniaxial crystals with different signs of the longitudinal and transverse components of the permittivity tensor [7]. Such dispersion also gives rise to

enhanced spontaneous decay rates of nearby emitters [8–10]. Hyperbolic metamaterials can be based on, e.g., arrays of vertically aligned nanorods [11] or layered metal-dielectric structures [8]. They have already been used to demonstrate improved resolution in linear optical microscopy [12–14]. These microscopy techniques, however, have not been able to address the demand for the lateral resolution required for optically thick (e.g., biological) sample analysis.

In both conventional and near-field microscopy, significant improvements can be achieved via intensity-dependent interactions [15,16]. Second-harmonic (SH) microscopy is a powerful tool enabling three-dimensional imaging with relatively high lateral resolution determined by the confinement of the fundamental-frequency light in either confocal or tip-enhanced configurations. It has been used in the visualization of cell membranes and even the whole biological organisms [17]. However, microscopic nonlinear interactions, being naturally inefficient, require high optical powers that could lead to photo-damage of samples, especially biological ones [18]. Moreover, in confocal-type second-harmonic generation (SHG) measurements, the signal is preferentially radiated in the far-field in directions where phase-matching conditions are fulfilled. Therefore, the information carried by other SH components, present in the near-field, is not recorded. The amount of information carried out by second-harmonic microscopy can be substantially increased using near-field scattering [19,20] or properly designed nanostructuring to engineer access to the evanescent (dark) SHG fields. Another example is second-harmonic microscopy with multilayer metal-dielectric stack, which enables to achieve subwavelength resolution due to suppression of the phase-locked SHG in properly configured geometries [21].

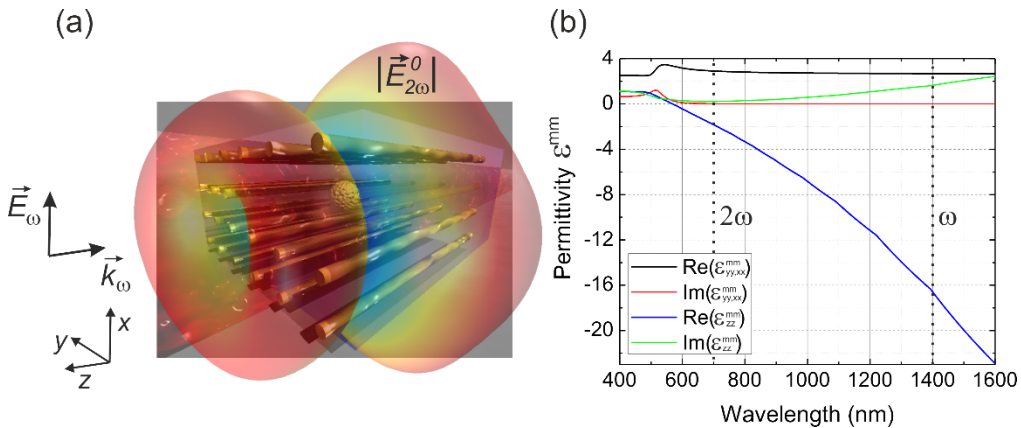


Fig. 1. (a) The general concept of nonlinear microscopy with a hyperbolic meta-antenna. The object (a spherical nanoparticle) is illuminated by a light at the fundamental frequency propagating in z direction and polarised along x direction. (b) Effective permittivity of the nanorod metamaterial (array of gold nanorods with 25 nm radius, 250 nm length and 100 nm periodicity, embedded in a dielectric fluid with $\epsilon_d = 2.25$).

Here, we propose an efficient metamaterial antenna operating in the hyperbolic dispersion regime as a novel approach for nonlinear optical microscopy providing access to evanescent, dark SH fields and converting them into propagating SH light (Fig. 1). We validate the concept numerically considering two complementary configurations. First, a second-harmonic generation from a nanoparticle is considered which directionality is modified by a metamaterial antenna. In the alternative realisation, second-harmonic generation from the metamaterial itself is used to track the position of a nanoparticle without any nonlinear response. A 10^3 -fold enhancement of the second harmonic signal from a spherical nonlinear nanoparticle embedded in the metamaterial antenna has been demonstrated in the first configuration. The far-field SH radiation pattern of the nanoparticle was shown to be

extremely sensitive to the position of the nanoparticle within the nanorod meta-antenna. The high sensitivity to the position of the nanoparticle makes the nonlinear optical microscopy presented here a novel promising high-resolution tool with applications in detection, tomography and tracking of nano-objects.

2. Numerical modelling

2.1 Linear optical properties of nanorod metamaterials

A hyperbolic metamaterials considered here is based on an array of metallic nanorods [Fig. 1(a)], the fabrication of which has been well established [22,23]. The homogenisation of such anisotropic metamaterial can be performed within an effective medium theory [24] valid for the nanorod radius less than the skin depth, as confirmed using finite element modelling (FEM). The effective medium theory (EMT) reveals that for frequencies below the effective plasma frequency [25], which depends on the geometrical parameters of the array and material properties of a metal and a dielectric, the metamaterial has opposite signs of the diagonal components of the effective permittivity tensor for light polarised along the nanorod axes ($\epsilon_{zz}^{mm} < 0$) and perpendicular to it ($\epsilon_{xx}^{mm}, \epsilon_{yy}^{mm} > 0$). Under these conditions, the metamaterial exhibits a hyperbolic dispersion [8]. In the context of this work, the metamaterial was designed with gold (Au) nanorods of 25 nm radius, 250 nm length and 100 nm periodicity embedded in a dielectric (e.g., fluid, $\epsilon_d = 2.25$) to have hyperbolic dispersion in the frequency range covering both fundamental and second-harmonic frequencies studied. The corresponding effective permittivity at the fundamental wavelength of 1400 nm are $\epsilon_{xx,yy}^{mm} = 2.67 + 0.0039i$ and $\epsilon_{zz}^{mm} = -16.6 + 1.4i$, while at the SH wavelength of 700 nm, $\epsilon_{xx,yy}^{mm} = 2.9 + 0.02i$ and $\epsilon_{zz}^{mm} = -1.8 + 0.2i$ [Fig. 1(b)].

2.2 Second-harmonic generation modelling

The numerical study of the SH emission was performed using a two-step procedure in the finite element model. In a first step, the field distribution induced by the fundamental wave is simulated to determine the local fields at the nanoparticle surface. Then, a second step uses the fields at the fundamental frequency to determine the nonlinear polarisability of the nanoparticle. This is done within the undepleted pump approximation (weak nonlinearity) and by introducing the surface polarisability phenomenologically. The resulting polarisation is then used as a source for the electromagnetic field at the second-harmonic frequency. In the context of this study, we pay particular attention to the radiation pattern corresponding to the far-field radiation profiles found via an analytical extrapolation of the fields in a domain surrounding the antenna using the Stratton-Chu approach [26].

3. Results

3.1 Nonlinear second-harmonic generation from the nanoparticle inside the metamaterial nanoantenna

To demonstrate the proposed concept of hyperbolic metamaterial antenna for the extraction of near-field second-harmonic information to the far-field, we have investigated, as a proof of principle, the SHG of a subwavelength spherical particle with second-order nonlinearity. The SH signal is assumed to originate from the nonlinear polarisation [27]

$$P_{2\omega,\perp} = \chi_{\perp\perp\perp} E_{\omega,\perp}^2 \quad (1)$$

where $\chi_{\perp\perp\perp}$ is a nonlinear susceptibility and $E_{\omega,\perp}(\omega)$ is the fundamental electric field component perpendicular to the particle's surface. In a uniform environment, the far-field SHG from centrosymmetric nanoparticles with such nonlinearity possesses mostly dipolar and

quadrupolar contributions [28–30]. However, the far-field signature of the dipolar field is extremely weak due to the symmetry of the nanoparticle, solely originating from retardation effects since the nonretarded contributions from opposite parts of the surface interfere destructively. The quadrupole contribution to SHG, on the other hand, is weak due to its low radiation efficiency.

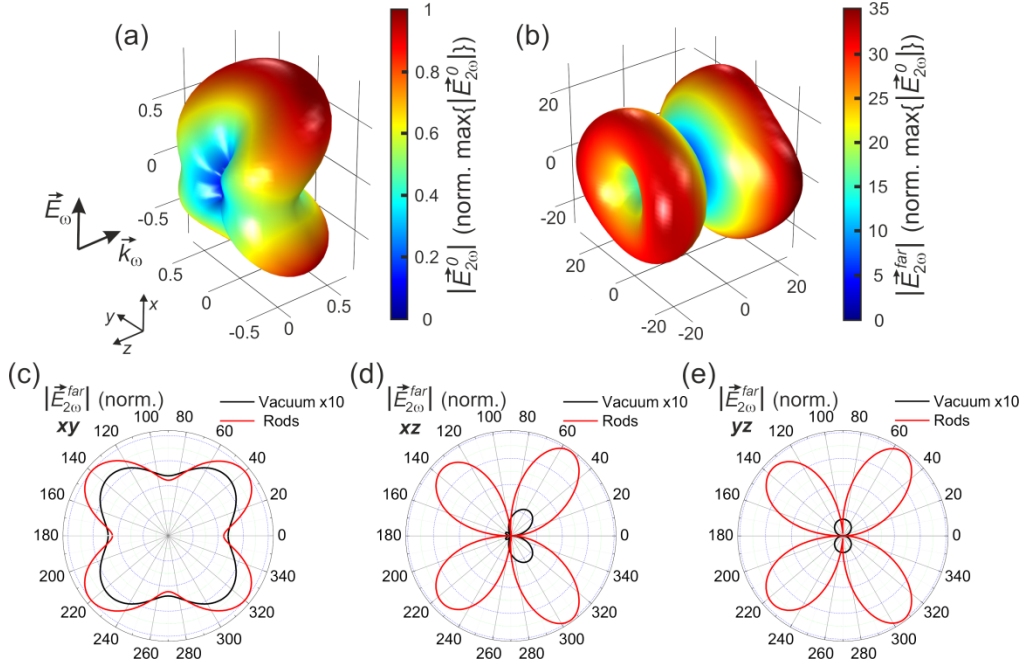


Fig. 2. SHG radiation patterns (plotted as the SH amplitude normalized to the maximum value of the SH from the particle placed in uniform dielectric $\max\{|E_{2\omega}^0|\}$) from a 10 nm diameter nonlinear particle in (a) uniform dielectric and (b) embedded in the metamaterial nanoantenna. (c–e) Cross-sections of the far-field radiation diagrams. Cutting planes are indicated above the polar plots: (black) the nanoparticle in free space and (red) the nanoparticle inside the metamaterial. The fundamental light is x -polarised. The metamaterial parameters are as in Fig. 1(b).

To increase the efficiency of the SH radiation, we propose to embed the nonlinear object in a hyperbolic metamaterial composed of an array of aligned plasmonic nanorods which exhibits hyperbolic dispersion at the second-harmonic frequency (Fig. 1). A nonlinear spherical particle (5 nm radius) was placed in the centre of 6×6 array of gold nanorods forming a $600 \times 600 \times 250 \text{ nm}^3$ meta-antenna. The fundamental light is a plane-wave with a wavelength of 1400 nm incident on the antenna along the direction of the nanorod main axis (z axis), and with a linear polarisation perpendicular to the rod's axis (x axis). As a result, the fundamental beam is an ordinary wave, corresponding to a positive component of the effective medium permittivity tensor ($\epsilon_{xx}^{mm} > 0$). The use of the 1400 nm excitation wavelength taken in this example, can be extended to any other wavelengths without loss in the generality of the results as long as the SH frequency is within the hyperbolic dispersion of the metamaterial. For the considered geometry, this corresponds to fundamental wavelengths above approximately 1000 nm.

The far-field directivity diagrams of the SHG from the nanoparticle in the hyperbolic antenna reveal patterns both qualitatively and quantitatively differing from those observed in free space (Fig. 2). In free space, both the retardation-induced dipolar SHG and a quadrupolar far-field signature [Fig. 2(a)] result in the same far-field profile as predicted by an analytical

theory [28,29], confirming the validity of the numerical approach used here. The compounded contributions from both SH contributions to the emission diagramme lead to the deformed ‘doughnut-like’ shaped far-field profile.

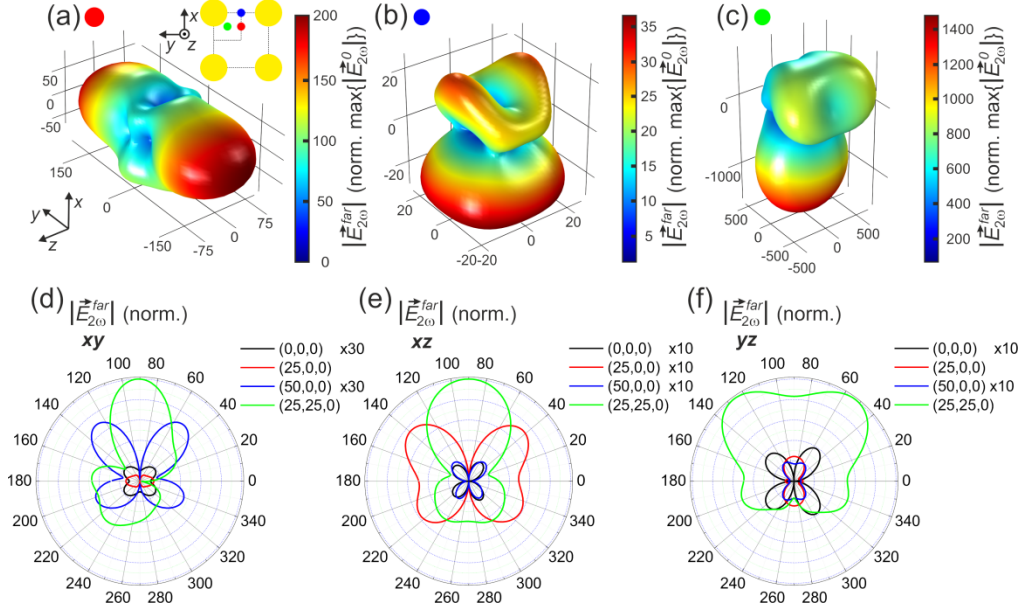


Fig. 3. (a) Far-field SHG radiation patterns (plotted as the SH amplitude normalized to the maximum value of the SH from the particle placed in uniform dielectric $\max\{|E_{2\omega}^0|\}$) for different positions of a nanoparticle inside the metamaterial antenna: (a) (25 nm, 0, 0), (b) (50 nm, 0, 0), and (c) (25 nm, 25 nm, 0). The coordinate origin is the centre of the unit cell. (d–f) Cross-sections of the far-field radiation diagrams in (a–c); the particle positioned at the origin (black), at (25 nm, 0, 0) (red), (50 nm, 0, 0) (blue), (25 nm, 25 nm, 0) (green). Cutting planes are presented above the polar plots. All other parameters are as in Fig. 2. The inset in (a) shows the considered particle positions, the size of the particle is enlarged for the visibility and is not to scale.

The introduction of the nanoparticle in the metamaterial antenna drastically changes the magnitude of the SH signal and the directionality of the radiation pattern [Fig. 2(b)]. In this environment, the SH field generated by the localised source inside the antenna couples to the modes with high wavevectors supported by the hyperbolic metamaterial antenna [25,31]. Inside the metamaterial, the SH intensity distribution follows the double-side conical shape expected for a point-like radiation source in a hyperbolic metamaterial [32] with the scattering on the metamaterial boundaries ultimately defining the far-field SH radiation pattern. The opening angle of the SHG polarisation cone, as estimated for an emitter situated in a homogeneous hyperbolic metamaterial, can be evaluated as $\theta^{mm} = \tan^{-1} \sqrt{\epsilon_{zz}^{mm} / |\epsilon_{xx,yy}^{mm}|} = 38^\circ$, using the effective permittivity of the infinite metamaterial at the SH frequency. This is in agreement with the cross-sectional analysis [Fig. 2(c)], where $\theta \cong 50^\circ$. The field pattern does not possess reflection symmetry with respect to the $z = 0$ plane, which is the result of the symmetry breaking due to the illumination conditions.

The overall far-field SHG intensity is also significantly increased when the nanoparticle is placed inside the metamaterial. The corresponding intensity enhancement is more than 1000-fold, due to both the enhancement of the fundamental field in the metamaterial, which provides a factor 100 enhancement in the SHG intensity, and by the enhanced scattering of the near-field SH described above [Fig. 2(b)]. As expected, the enhancement at the

fundamental and SH frequencies contribute unequally to the overall efficiency, since the SHG depends quadratically on the field amplitude at the fundamental frequency.

3.2 Super-resolution with second-harmonic microscopy with nanorod metamaterial

In order to evaluate the spatial resolution of this nonlinear technique, the nanoparticle's position inside the unit cell of the array was varied while monitoring the evolution of the far-field SHG radiation pattern. Clear far-field detectable features of the SHG distribution, sensitive to transverse shifts in the nanoparticle's position as small as 5 nm, can be detected [Figs. 3(a)–3(c)]. In particular, the SHG intensity differs by orders of magnitude in specific directions for different positions of the particle within the meta-antenna. Such remarkable sensitivity results from a strong position-dependent near-field interaction between the particle and the structured geometry of the metamaterial at both fundamental and second-harmonic frequencies. Here, the nanostructured environment provides access to evanescent SH fields generated by the object through a position-dependent field enhancement. Furthermore, the SHG signal is particularly intensified when the symmetry between the excitation of nonlinear sources at the opposite sides of the nonlinear nanoparticle is broken, leading to a dramatic increase of the dipole SHG contribution [cf. positions (50 nm, 0, 0) and (25 nm, 25 nm, 0) in Figs. 3(b) and 3(c)]. As a consequence, the nanostructured metamaterial acts as an antenna for the SH signal generated by the embedded nanoparticle, enhancing and redirecting the SHG signal with an efficiency governed by the position of the nanoparticle relative to the nanorods within the hyperbolic metamaterial. Monitoring both the intensity of the SH signal and the SHG radiation pattern allows determining the geometrical arrangement, ultimately leading to the possibility of tracking the nanoparticle trajectory relative to the antenna down to a few nanometres resolution.

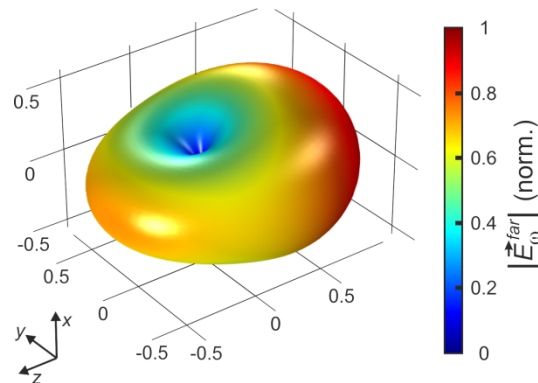


Fig. 4. Far-field scattering from the nanoparticle in the meta-antenna at the fundamental 1400 nm wavelength. All other parameters are the same as in Fig. 1. The scattering pattern is the same within 1% error for all the positions of nanoparticle considered in Fig. 3.

To compare the SHG-based tracking performance to its linear counterpart, the far-field radiation pattern at the fundamental frequency was analyzed (Fig. 4). It was found that for all four analyzed particle positions, the linear scattering patterns differ by no more than 1% in the radiated field in any directions, making the linear scattering approach impractical for tracking purposes and underlining the superiority of the SH approach. The difference between linear and SHG sensitivities comes from the fact that in the linear regime the antenna scattering dominates the far-field pattern, and, therefore, the scattering from the nanoparticle, which is essentially insensitive to the position-defined local field enhancement does not play a significant role.

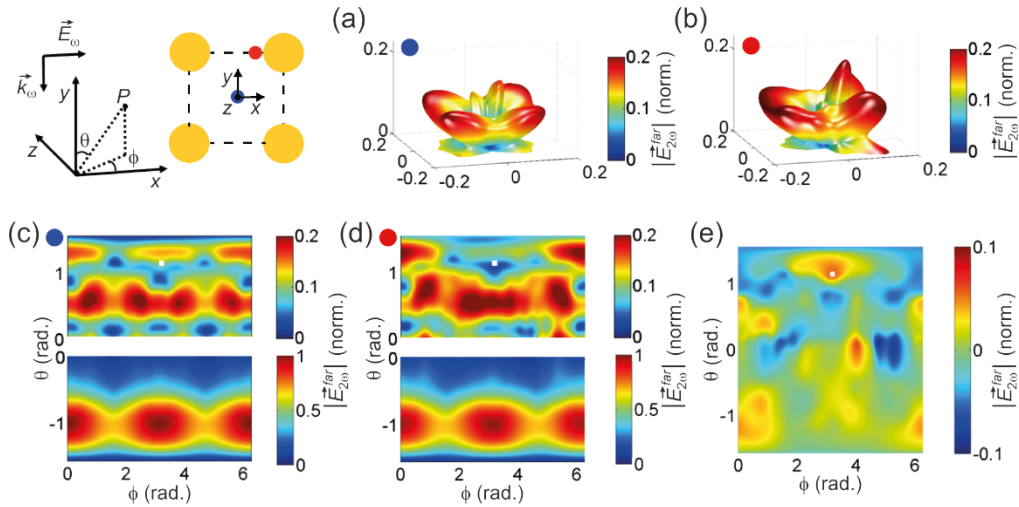


Fig. 5. Far-field SHG radiation patterns from a 400 nm-diameter metamaterial region containing a metallic nanoparticle in the central unit cell. The nanoparticle is located (a,c) in the centre of the unit cell and (b,d) 1 nm down from the surface of top-right rod of the unit cell. (c,d) Difference between the SHG signals from (a,d) and (b,e). The white square in (c-d) at the position $(\phi = 184^\circ, \theta = 66^\circ)$ indicates the direction where the SHG intensity change is 60%. The inset shows the considered particle positions, the size of the particle is enlarged for the visibility and is not to scale.

3.3 Nanoparticle-scattered SHG from nanorod metamaterial

We now consider a complementary scenario and study how a nanoparticle without nonlinear response changes the SHG from the metamaterial made of nanorods possessing second-order nonlinear susceptibility. In this case, the surface nonlinearity of individual Au nanorods forming the metamaterial is also considered to be given by Eq. (1). Other nonlinear surface and bulk sources were previously considered for the case of Au nanorods and nanospheres, and it was found that the SH emission is dominated by the orthogonal surface term [33,34]. A plane wave was incident on a 16×16 nanorod array (with same size and optical properties as the metamaterial antenna considered above). To avoid field singularities at the edges of the nanorods, the rod's extremities were rounded, so that they have spherical tips [31]. (The edge effects are much less important in the linear response of nanorods and the rounding was not considered in Sections 3.1 and 3.2.) A SHG signal from a metamaterial region of a diameter of 400 nm centred at the unit cell where the nanoparticle is located was considered. This mimics the collection of the SHG signal from a $\sim \lambda/2$ -wide region in a confocal microscopy configuration. Thus, the signal from 12 neighbouring nanorods was considered. When the nanoparticle is located at the centre of the cell [Figs. 5(a) and 5(c)], no modifications of the SHG signal from the metamaterial are practically detected. However, when the nanoparticle is placed 1 nm away from the surface of a nanorod (point with coordinates (19 nm, 50 nm, 0)), a drastic modification of the far-field radiation diagram is observed [Figs. 5(b) and 5(d)]. For the observation angles $\phi = 184^\circ$ and $\theta = 66^\circ$, a maximum nanoparticle-induced change of the SHG signal generated by the metamaterial is almost $\max \left(\left| \vec{E}_{2\omega, 1\text{nm}}^{\text{far}} \right| - \left| \vec{E}_{2\omega, \text{cent}}^{\text{far}} \right| \right) / \left| \vec{E}_{2\omega, \text{cent}}^{\text{far}} \right| = 60\%$ in intensity [Fig. 5(e)].

4. Conclusion

The concept of hyperbolic metamaterial nanoantenna was introduced and exemplified for high-resolution nonlinear optical microscopy and tomography. The use of such an antenna was shown to increase the far-field SH radiation intensity of a 10 nm diameter nonlinear

nanoparticle by 3 orders of magnitude compared to the same particle placed in a uniform dielectric, with a strong dependence of the enhancement and radiation pattern on the nanoparticle's position. The enhancement is related to both the local field enhancement in the metamaterial and its ability to convert dark evanescent SH field components generated by the nanoparticle into propagating modes, detectable in the far-field. The observed far-field SH radiation pattern has distinctive directional features which were found to be extremely sensitive to the nanoparticle's position with respect to the antenna, a feature that can be used to track the position of the SH source within the antenna with a nanometre scale resolution. The complementary phenomenon was also demonstrated for a spherical nanoparticle without nonlinear response placed in a nonlinear metamaterial nanoantenna, leading to a 60% change in the directionally emitted SH. The proposed hyperbolic metaparticle based antennas, can be straightforwardly fabricated [23] and their use can be generalized to study any nanoscale systems and phenomena supporting dark photonic modes. The development of highly nonlinear nanoscale optical components also hold a great potential for future integrated nano-opto-electronic devices where traditional nonlinear crystals cannot be used due to the phase-matching conditions.

Acknowledgments

This work was supported, in part, by EPSRC (UK), the ERC iPLASMM project (321268), US Army Research Office (W911NF-12-1-0533 and W911NF-13-1-0282). A.V.Z. acknowledges support from the Royal Society and the Wolfson Foundation. G.A.W. acknowledges support from the EC FP7 project 304179 (Marie Curie Actions). The data access statement: all data supporting this research are provided in full in the results section.